16th Australasian Fluid Mechanics Conference
Crown Plaza, Gold Coast, Australia
2-7 December 2007

The effect of corrugation height on flow in a wavy-walled pipe

H. M. Blackburn[1], A. Ooi[2] and M. S. Chong[2]

[1]Department of Mechanical Engineering
Monash University, Victoria, 3800 AUSTRALIA

[2]Department of Mechanical and Manufacturing Engineering
The University of Melbourne, Victoria, 3010 AUSTRALIA

Abstract

We have used direct numerical simulation to examine both laminar and turbulent flows in circular pipes with smoothly corrugated walls, where the corrugation wavelength has been kept constant at $0.419D$, and the corrugation height was varied from zero to $0.08D$. Flow rates have been varied in steps between low values that provide laminar flow, up to higher values where the flow is turbulent: the maximum bulk flow Reynolds number for the smooth pipe was $Re_D = UD/\nu = 10\times10^3$, giving a friction Reynolds number $Re_\tau = 314$. Even in the laminar regime, the larger corrugation heights produce flow separation, and the proportion of pressure drop that is attributable to pressure drag can be of order 50%, rising to approx 85% in turbulent flow. In turbulent flow, near-wall structure is heavily influenced by the effects of flow separation and reattachment. However, further from the wall, statistics show standard outer-flow scaling relationships, indicating that (as for standard roughness treatments) the outer flow is mainly affected by the value of wall drag, rather than details of the wall shape. In addition to supplying more detail on the above, we provide friction factor vs. bulk flow Reynolds number values that compare our results with Nikuradse's classic sand-roughened pipe flow data.

Introduction

There is now a reasonable amount of published direct numerical simulation (DNS) data available for canonical turbulent flows: two-dimensional channel, circular pipe, flat plate boundary layer, backward-facing step. However, despite the practical importance of rough-walled turbulent flows (since all real surfaces are 'fully rough' when Reynolds numbers are sufficiently high) few simulation studies exist that attempt to quantify turbulent flows where the wall is roughened in any way. The present work seeks to make a contribution by carrying out flow simulations in a circular pipe with smoothly corrugated walls, where the streamwise wavelength of the corrugations is long (hundreds of wall units), and the corrugation amplitude is a variable parameter.

All the domains under consideration have the same mean radius $\bar{R} = D/2$, and (for turbulent flow calculations) the same axial length $L = 2\pi D$. As is common in simulations of this type, the flow has been assumed periodic in the axial direction, and a body force is used to drive the flow, allowing the pressure to remain periodic also. The length:diameter ratio was chosen on the basis that previous pipe-flow DNS for $L = 5D$ [5] has established that the absolute values of axial two-point correlation coefficients for velocity were below 0.1 over the whole radius at an axial separation of $2.5D$, and for $Re_D = 5000$. This result suggests that at $L = 2\pi D$ the domain is long enough to remove most of the correlation associated with large-scale turbulent structure, which scales on the diameter.

For the wavy-wall geometries, 15 wavelengths were chosen over the domain length of $2\pi D$. With a peak-to-peak corrugation height h the radius of the pipe, $R(z)$, where z is the axial coordinate, is given by $R(z)/D = 0.5 + 0.5h\cos 15z/D$. (For laminar-flow calculations conducted at Reynolds numbers below transition, only a single module of the axial wave was represented, i.e. the domain length was reduced to $L_m = 2\pi D/15 \approx 0.419D$.) We note that since the wavelength is fixed, but the wave-height of the corrugations is varied, the corrugations of different height employed here are not geometrically similar.

The highest bulk-flow Reynolds number for the present data set is $Re_D = UD/\nu = 4\langle Q\rangle/\pi D\nu = 10\times10^3$, for the pipe with smooth walls. In order to establish basic parameters for turbulent flows, the Blasius friction factor correlation for smooth pipes [3],

$$\lambda = 4\tau_0/0.5\rho U^2 = 0.3164/{Re_D}^{1/4} \tag{1}$$

is used to estimate the wall shear stress τ_0, the friction velocity $u_\tau = (\tau_0/\rho)^{1/2}$, and the body force required to drive the flow. From equation (1), we can derive the smooth-pipe relationship

$$Re_\tau = u_\tau/\nu = 99.436\times10^{-3}{Re_D}^{7/8}, \tag{2}$$

and find that for $Re_D = 10\times10^3$, $Re_\tau = 314.4$. From the definitions above, we also have the relationship

$$\lambda = 32\left(Re_\tau/Re_D\right)^2, \tag{3}$$

which means that for a given body force (i.e. Re_τ), $\lambda \propto {Re_D}^{-2}$.

There is a minor complication arising from the fact that the ratio of surface area to volume for a wavy-walled pipe is not constant as corrugation-height h is varied. Using Pappus' Second Theorem, the domain volume can be found in closed form as $\pi(\bar{R}^2 + h^2/8)L$, provided the length comprises an integral number of wavelengths. The surface area of the domain has to be found numerically, as while Pappus' First Theorem holds, the arc length of the curve that describes the maximum radius is not available in closed form. When attempting to define both the bulk flow and friction Reynolds numbers for the wavy walled pipe, one needs an equivalent diameter. For simplicity, we have adopted the mean diameter $D = 2\bar{R}$ for this measure. Using this equivalent diameter, an equivalent mean wall shear stress is found by equating the mean wall tractive force to the body force on the domain, i.e.

$$2\pi L\bar{R}\bar{\tau}_w = \rho\pi\left(\bar{R}^2 + h^2/8\right)Lg, \tag{4}$$

where g is an axially directed body force per unit mass, from which

$$u_\tau^2 = \frac{\tau_w}{\rho} = \frac{\bar{R}}{2}\left(1 + \frac{h^2}{8\bar{R}^2}\right)g \tag{5}$$

With this choice of equivalent diameter, if one wishes to keep the friction velocity and hence $Re_\tau = u_\tau\bar{R}/\nu$ constant, the driving force per unit mass g must be reduced as h (and hence, the volume of the domain, V) increases according to

$$g(h) = g_0V_0/V = g_0/(1 + h^2/8\bar{R}^2). \tag{6}$$

Label	$h^+_{10^4}$	h/D	$R_{\min}/D$	V/V_0	S/S_0
A	0	0.00000	0.50000	1.00000	1.00000
B	5	0.00795	0.49602	1.00003	1.00794
C	10	0.01590	0.49205	1.00013	1.01533
D	20	0.03181	0.48410	1.00051	1.03186
E	30	0.04771	0.47615	1.00114	1.04788
F	40	0.06361	0.46819	1.00202	1.06397
G	50	0.07952	0.46024	1.00316	1.08013

Table 1: Summary of wavy walled geometric parameters. $h^+_{10^4}$ is the peak–peak corrugation height expressed in wall units at $Re_D = 10 \times 10^3$. V/V_0 is the domain volume normalised by that for the smooth pipe (case A). S/S_0 is the domain surface area normalised by that for the smooth pipe.

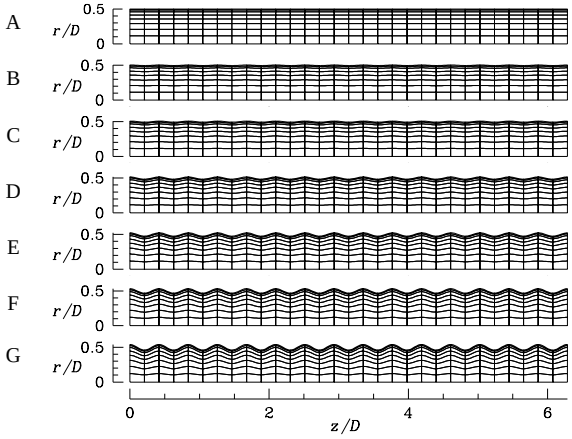

Figure 1: Spectral element meshes, each with 240 elements in the meridional semiplane. Labels match those used in table 1: A, smooth-walled pipe; B, $h^+_{10^4} = 5$; C, $h^+_{10^4} = 10$; D, $h^+_{10^4} = 20$; E, $h^+_{10^4} = 30$; F, $h^+_{10^4} = 40$; G, $h^+_{10^4} = 50$.

Here, V_0 is the volume of the smooth-walled pipe and g_0 is the corresponding axial driving force.

The maximum corrugation peak–peak amplitude of $h/D = 0.07952$ was chosen to be 50 wall units at $Re_D = 10 \times 10^3$, i.e. $h^+_{10^4} = 50$. Simulations have also been carried out for lower corrugation heights of 40, 30, 20, 10, 5 and 0 wall units (all normalised at $Re_D = 10 \times 10^3$). Table 1 summarises the main parameters of the wavy-walled geometries used in the present study. It can be seen that the fractional increase in volume V/V_0, and hence the fractional reduction in driving force, is less than half a percent even at the largest corrugation height, case G. The corrugation wavelength, $L_m = 2\pi D/15$, corresponds to 263.4 wall units at $Re_D = 10 \times 10^3$.

Discretisation

The simulations have been carried out with a spectral element/Fourier discretisation (Fourier expansions are employed in the azimuthal coordinate, spectral elements in the meridional semi-plane). The method has exponential/spectral convergence in all coordinates [2], and has previously been used for DNS of turbulent flows in smooth-walled pipes [7]. Three-dimensional simulations are parallelised across Fourier planes. Outlines of the 240-spectral-element-meshes for cases A–G are shown in figure 1. Our mesh design strategy for resolution of near-wall flows is described in [1].

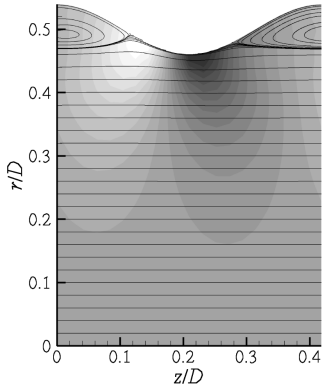

Figure 2: Streamlines and contours of pressure (dark grey represents low pressure) for laminar flow at $Re_\tau = 78.6$, geometry case G. Since the flow is laminar and steady, only a single module of the wavy wall is represented in the laminar flow calculations.

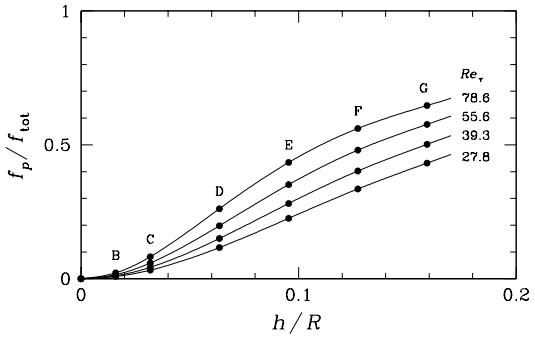

Figure 3: Pressure drag as a proportion of total wall drag as a function of h/R for different wall Reynolds numbers in laminar flow.

Laminar Flow

In the current set of simulations, initially turbulent flows are found to relaminarise and become steady for $Re_\tau \leq 78.6$, and we have computed laminar flows down to $Re_\tau = 27.8$. In order to reduce computational load, these simulation are treated as axisymmetric and only a single module of corrugation is represented, as shown in figure 2. The flow tends to remain attached at the lower corrugation heights and at lower Reynolds numbers: at $Re_\tau = 27.8$, cases F and G exhibit detachment (F only marginally), while at $Re_\tau = 78.6$ cases D–G exhibit detachment (D marginally). In figure 2 (case G, $Re_\tau = 78.6$), flow streamlines clearly show recirculation at radii greater than the minimum. Also one can see that around the reattachment stagnation zone there are significantly elevated pressures; owing to nonlinearity the pressure near the detachment point is not similarly elevated and this imbalance leads to a significant contribution of pressure drag, in addition to viscous drag: the relative contributions are shown for all corrugation heights and laminar Reynolds numbers in figure 3. It can be seen that, as for flow separation, the relative contribution of pressure drag increases both with corrugation height and Reynolds number.

Figure 4 shows velocity profiles at the minimum radial location (for $z/D \approx 0.2095$ in figure 2) for all corrugation heights at $Re_\tau = 55.6$. The axial velocity u is normalised by the bulk (area average) speed U, and the radial coordinates in each case

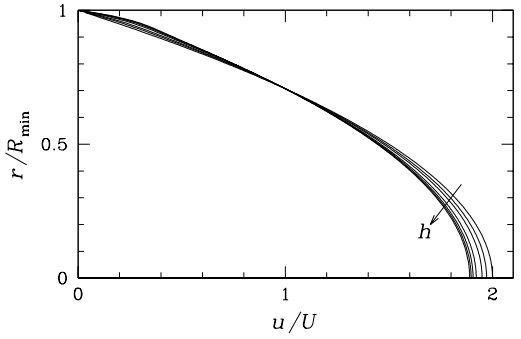

Figure 4: Velocity profiles at minimum pipe radius for laminar flow at $Re_\tau = 55.6$. Normalising velocities are calculated from the volume flow rate and the cross-sectional area at minimum radius, R_{min}. Arrow indicates increasing corrugation-height, h.

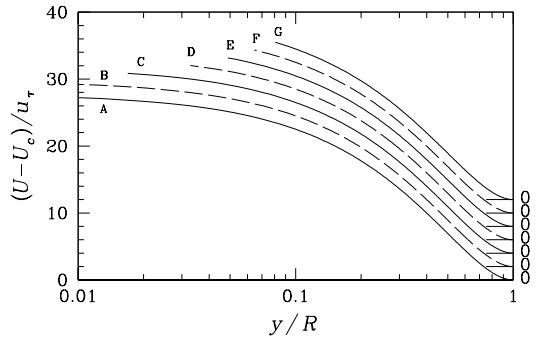

Figure 5: Normalised velocity defect $(U-U_c)/u_\tau$ for different corrugation-heights h in laminar flow, $Re_\tau = 55.6$. Geometry case labels as for figure 1. Note that cases for different corrugation height are offset vertically of clarity.

are normalised by R_{min}. The smooth-wall case is parabolic and has $u/U(r=0) = 2$ as expected for Poisueille flow in a straight pipe. As corrugation height h increases, the flow near the wall at R_{min} speeds up relative to a parabolic profile, and so the normalised centreline velocity falls to compensate. However, the shape of the velocity profiles near the pipe centreline remain closely parabolic in all cases.

Figure 5, which shows the axial-average velocity defect profiles, emphasises that while wall corrugation obviously affects the flow near the wall, nearer the centre of the pipe the effect is insignificant. (The figure is plotted in log-linear format to aid comparison with the forthcoming equivalent plot for turbulent flow, figure 9.)

The Blasius (a.k.a. Darcy–Weisbach) friction factor is shown as a function of bulk-flow Reynolds number in figure 6 for the laminar flow cases. It can be seen that the friction factor increases with corrugation height at all Reynolds numbers represented, although the relative increase falls with Reynolds number. These characteristics are in accord with remarks made above regarding figure 3. As expected, the smooth-wall cases give $\lambda = 64/Re_D$ to very good accuracy.

Turbulent Flow

Now we turn to examine turbulent flow results, initially concentrating on data for the highest friction Reynolds number $Re_\tau = 314$ (corresponding in the smooth pipe to $Re_D = 10\times10^3$).

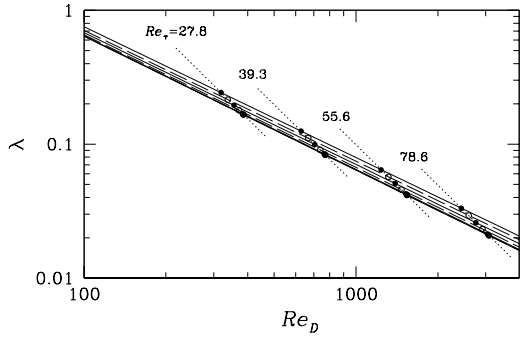

Figure 6: Pipe friction factor λ as a function of Re_D for laminar flows at four different values of Re_τ. In each set, the lowest value of λ corresponds to the smooth pipe, case A (where $\lambda = 64/Re_D$), the upper point to case G.

Validation of Smooth-Wall Simulation at Re_τ=314

In order to help build confidence in the veracity of the turbulent flow calculations, we show in figure 7 a comparison of first- and second-moment statistics obtained in our computations to LDA-based experimental results obtained at $Re_D = 10\times10^3$ (i.e. $Re_\tau = 314$) [4]. Agreement for the mean-flow profile is excellent and generally the agreement for all statistics presented is very good except in the near-wall region where inaccuracies in the experimental estimates of fluctuating axial and radial velocities are evident. Our fit to the presumed log-law section of the mean velocity profile gives

$$U^+ = \frac{U}{u_\tau} = \frac{1}{\kappa}\ln\frac{u_\tau y}{\nu} + C = 2.5\ln y^+ + 5.4, \qquad (7)$$

i.e. a von Kármán constant $\kappa = 0.40$ and a log-law offset $C = 5.4$.

Turbulent Flow Data at Re_τ=314

Figure 8 shows the mean-flow velocity profiles at $Re_\tau = 314$ for all corrugation heights. Note that as corrugation-height increases, these profiles commence at progressively greater values of y^+, since the minimum sensible radius at which to begin averaging, R_{min}, becomes progressively smaller, whereas the distance from the wall, y, is calculated as beginning on the mean radius, $\bar{R}$. Maximum centreline velocities fall with increasing corrugation height, as expected, however the shape of the velocity profiles near the centreline remains substantially the same. The similarity of the velocity profiles near the centreline is emphasised by plotting them as velocity-defect profiles, shown in figure 9.

The offset in the mean velocity profiles can be estimated by plotting $U/u_\tau - \kappa^{-1}\ln y^+$ vs. y^+, where log-law segments of mean velocity profiles will appear as horizontal lines whose ordinate corresponds to the log-law constant C. This procedure and the corresponding values of C for all corrugation heights are illustrated in figure 10.

A simple (but admittedly slightly imprecise) means of assessing the presence or otherwise of mean flow separation is to compute the mean viscous wall traction at minimum and maximum pipe radii. This can be accomplished by differentiating the mean flow velocity profiles, with outcomes for $Re_\tau = 314$ shown in figure 11. Evidently, flows for geometries A–C remain attached on average, since the viscous wall traction does not become negative. Perhaps surprisingly, this is quite similar to the maximum-Re_τ result for laminar flow, see above.

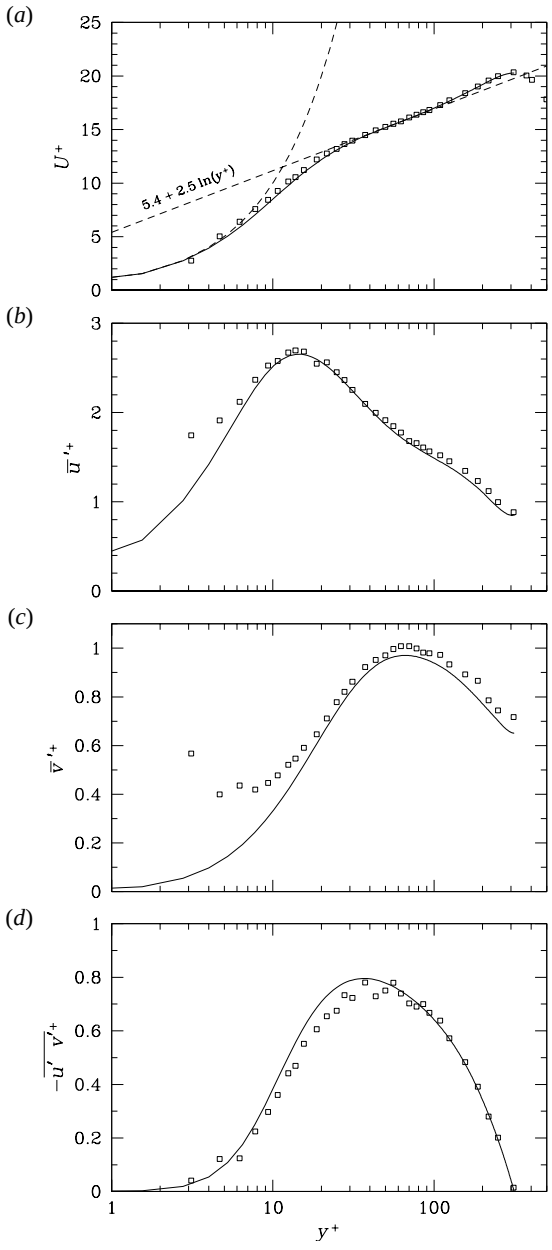

Figure 7: Comparison of flow profile data for the smooth-walled pipe at $Re_D = 10 \times 10^3$ (solid lines) with LDA-based values [4] (squares). (*a*), mean flow, with dashed lines for linear sublayer and fitted log law; (*b*), rms axial velocity fluctuation; (*c*), rms radial velocity fluctuation; (*d*), Reynolds shear stress.

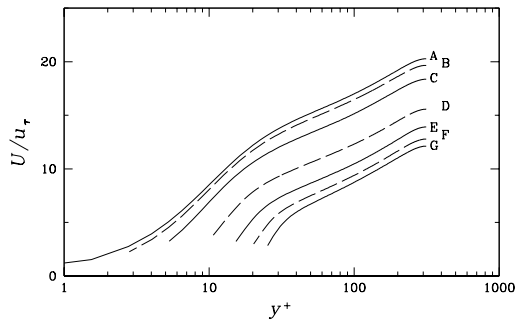

Figure 8: Mean-flow law-of-the-wall velocity profiles at $Re_\tau = 314$ for different corrugation-height cases.

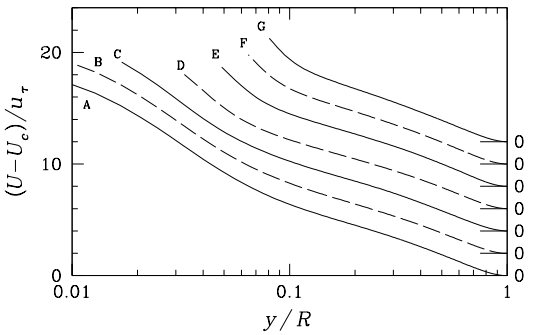

Figure 9: Normalised velocity defect $(U - U_c)/u_\tau$ for different corrugation-heights h in turbulent flow, $Re_\tau = 314$. Note that cases for different corrugation height are offset vertically of clarity. Cf. figure 5.

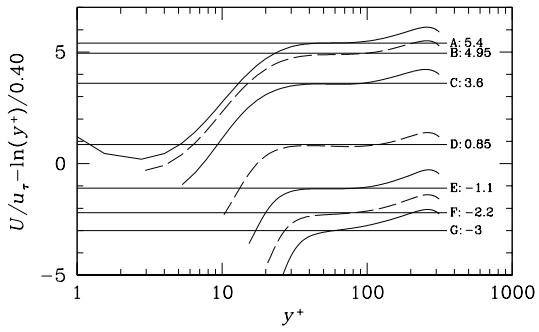

Figure 10: Correction constant in the logarithmic law-of-the-wall for different corrugation-height cases at $Re_\tau = 314$, on the assumption that the log-law slope constant is 0.40.

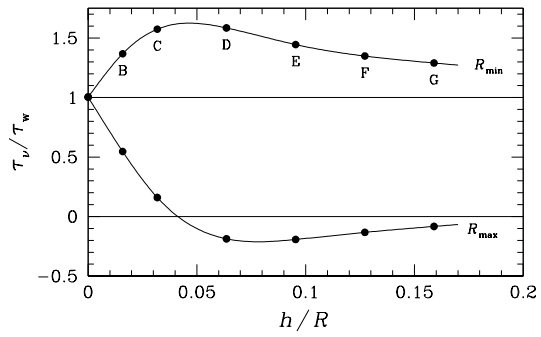

Figure 11: Mean-flow viscous wall traction at minimum and maximum pipe radii for different corrugation-heights at $Re_\tau = 314$. Values are normalised by the mean traction, τ_w, and are obtained by differentiating the mean-flow profiles.

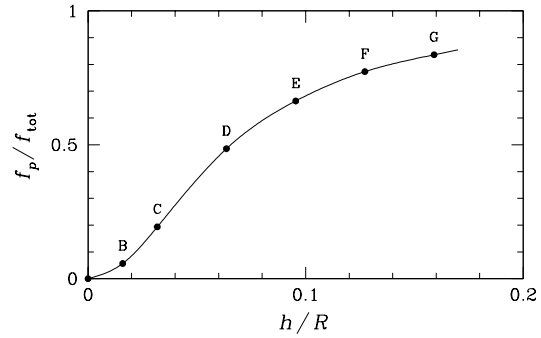

Figure 12: Pressure drag as a proportion of total wall drag as a function of h/R for turbulent flow at $Re_\tau = 314$. Cf. figure 3.

It may initially seem paradoxical that the absolute values of the departure of the minimum-R and maximum-R viscous wall traction shown in figure 11 from τ_w first increase, then decrease with increasing corrugation height. However, this mainly reflects the increasing relative importance of the pressure component of average wall drag, as illustrated for turbulent flow in figure 12. The overall contribution of pressure drag at the maximum corrugation height, case G, is quite large, approximately 85%, indicating that the flow is approaching full-rough (where by definition all the drag derives from pressure differences).

Comparison to Nikuradse's Roughened-Pipe Data

While a smoothly corrugated wall would not normally be accepted as 'rough', and certainly has no degree of geometric randomness, it is interesting to attempt to assess the equivalent sand roughness of our geometries. The standard comparison in this case is to Nikuradse's classic 1933 experimental data [6], obtained by glueing sand of different narrow-band size distributions to the inside of smooth circular pipes. Two exactly equivalent measures of the effect of sand roughness can be obtained from the log-law offset C (equation 7) and Nikuradse's 'roughness function'

$$B = C + \kappa^{-1} \ln k^+, \tag{8}$$

where the dimensionless sand roughness height $k^+ = u_\tau k/\nu$, k being the characteristic sand size. Nikuradse found that in the 'fully rough' regime where λ becomes independent of Re_D (alternatively Re_τ) and is only a function of k^+, the roughness function asymptotes to $B = 8.5$: equivalently the log-law offset

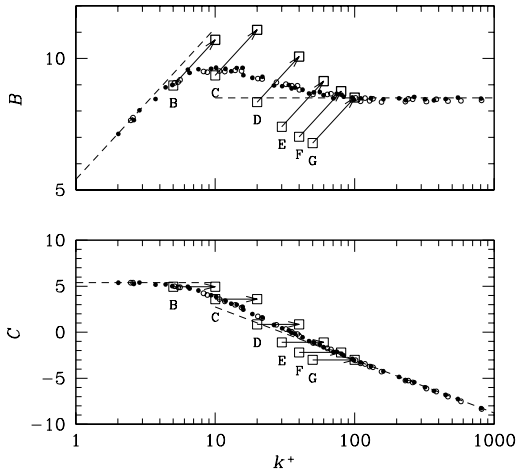

Figure 13: Nikuradse's data [6] for roughness function B and log-law correction constant C as functions of dimensionless sand roughness height k^+. Data for the corrugated wall at $Re_\tau = 314$ are also shown (cf. figure 10), both in raw state, and corrected to an equivalent sand roughness height.

$C \to 8.5 - \kappa^{-1} \ln k^+$. Nikuradse's data for B and C are plotted as small open and closed circles in figure 13. The two asymptotic values for large k^+ are shown as dashed lines (and at low k^+ another set of dashed lines indicate the smooth-pipe asymptotes for $C = 5.4$ and $\kappa = 0.40$).

Our data, derived from the log-law offsets at $Re_\tau = 314$ (see figure 10). and initially assuming that $h \equiv k$, are plotted on figure 13 as thin-lined open squares, labelled B–G. The values for both roughness measures B and C fall below Nikuradse's data for sand roughness, indicating that the wavy wall of given height has a greater effect in reducing mean flow rate than a coating of sand of equivalent size. This makes sense physically, since after some consideration one may well accept that an organised corrugation of given height could have more effect in disrupting near-wall flows than a random array of sand of equivalent size.

A question that arises is: by what factor does one need to multiply the corrugation height h in order to make the functions B and C agree with Nikuradse's data? Naturally, the validity of this process is open to debate, not least because our maximum Reynolds numbers fall well below Nikuradse's. Nevertheless, on the assumption that the data at the greatest corrugation heights are approaching 'fully rough' (and this does not seem too unreasonable on the basis of their raw k^+ values), we find that the correction factor which makes our high-corrugation-height data and Nikuradse's coincide is approximately 2.0. The corrected values of B and k^+ derived from our data are indicated by thick-lined open squares on figure 13, with arrows to indicate the amounts by which the raw data are shifted to obtain the corrected 'equivalent sand roughness' values.

As a further comparison to Nikuradse's data set, we show in figure 14 our values of friction factor λ vs. Re_D for geometries B–E from $Re_\tau = 314$ and at successively lower Re_D down into the laminar regime (where only values for case E are shown in order to avoid clutter). Nikuradse's data for different relative roughnesses R/k are shown as small open circles. It is interesting to note that the bulk flow Reynolds number for the onset of transition from laminar to turbulent flow, $Re_D \sim 2500$, is much the same in both data sets and indeed that the transitional value of λ for case E falls within the scatter band of Nikuradse's data.

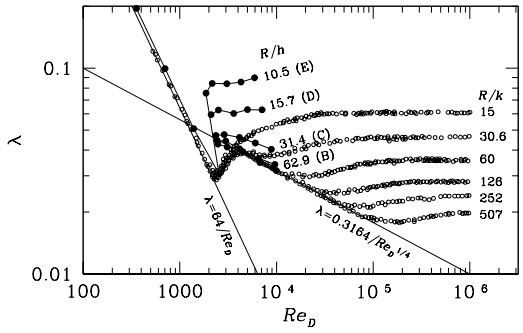

Figure 14: Nikuradse's data [6] for pipe friction factor as functions of Re_D and relative roughness R/k (open circles). Also shown is the variation of friction factor with Re_D for the corrugated wall at various Re_τ, computed for cases B–E (filled circles), together with the relative corrugation height R/h.

Transition to turbulence appears to occur much more rapidly with changing Re_D for the corrugated wall cases than for sand roughness. (We note that while asymptotic stability analysis shows that smooth-wall pipe flow is not linearly unstable at any Reynolds number, this may not be true for flow in pipes with corrugated walls.)

In the turbulent regime the values of λ for our simulations are comparable in magnitude to Nikuradse's at similar values of R/h and R/k, but it is difficult to draw firm conclusions. If one accepts the logic outlined above for the correction of corrugation height to equivalent sand roughness, then one would expect our data for $R/h = 62.9$ (case B) to eventually, with increasing Re_D, asymptote close to Nikuradse's data for $R/k = 30.6$, likewise our data for $R/h = 31.4$ to asymptote near Nikuradse's data for $R/k = 15$. Evidently further work is needed, but it is unlikely that full resolution of these issues can be provided by DNS alone in the foreseeable future.

Conclusions

For both laminar and turbulent flows in pipes with smooth corrugated walls, the outer mean flow (near the pipe centreline) appears unable to sense the detail of wall corrugation, only its effect on wall friction at any bulk flow rate. As wall corrugation height increases, pressure drag makes an increasingly large contribution to the total friction, even in the absence of (mean) flow separation, and in laminar as well as turbulent flow. At the highest Re_τ considered, and for the largest corrugation heights, we have estimated that an equivalent sand roughness can be obtained by multiplying the corrugation height by a factor of approximately two.

Acknowledgements

We would like to acknowledge support of APAC's Merit Allocation Scheme under grant D77. Thanks also to Jaap den Toonder for provision of smooth-wall experimental data.

References

[1] Blackburn, H. M. and Schmidt, S., Spectral element filtering techniques for large eddy simulation with dynamic estimation, *J. Comput. Phys.*, **186**, 2003, 610–629.

[2] Blackburn, H. M. and Sherwin, S. J., Formulation of a Galerkin spectral element–Fourier method for three-dimensional incompressible flows in cylindrical geometries, *J. Comput. Phys.*, **197**, 2004, 759–778.

[3] Blasius, H., Das Ähnlichkeitsgesetz bei Reibungsvorgängen in Flüssigkeiten, *Forschg. Arb. Ing.-Wes.*, **134**.

[4] den Toonder, J. M. J. and Nieuwstadt, F. T. M., Reynolds number effects in a turbulent pipe flow for low to moderate *Re*, *Phys. Fluids*, **9**, 1997, 3398–3409.

[5] Eggels, J. G., Unger, F., Wiess, M. H., Westerweel, J., Adrian, R. J., Friedrich, R. and Nieuwstadt, F. T. M., Fully developed turbulent pipe flow: A comparison between direct numerical simulation and experiment, *J. Fluid Mech.*, **268**, 1994, 175–209.

[6] Nikuradse, J., Strömungsgesetze in rauhen Rohren, *Forsch. Arb. Ing.-Wes.*, **361**, reprinted as NACA TM-1292, 1950.

[7] Schmidt, S., McIver, D. M., Blackburn, H. M. and Nathan, G. J., Spectral element based simulation of turbulent pipe flow, in *14th A/Asian Fluid Mech. Conf.*, Adelaide, 2001.

16th Australasian Fluid Mechanics Conference
Crown Plaza, Gold Coast, Australia
2-7 December 2007

Eigen-analysis of Inviscid Fluid Structure Interaction (FSI) Systems with Complex Boundary Conditions

A. D. Lucey and M. W. Pitman

Fluid Dynamics Research Group
Curtin University of Technology, Western Australia, 6845 AUSTRALIA

Abstract

A method for extracting the eigenvalues and eigenmodes from complex coupled fluid-structure interaction (FSI) systems is presented. The FSI system under consideration in this case is a one-sided, inviscid flow over a finite-length compliant surface with complex boundary conditions, although the method could be applied to any FSI system. The flow is solved for the inviscid case using a boundary-element method solution of Laplace's equation, while the finite compliant surface is solved through a finite-difference solution of the one-dimensional beam equation. The crux of the method lies in reducing the coupled fluid and structural equations down to a set of coupled linear differential equations. Standard Krylov subspace projection methods may then be used to determine the eigenvalues of the large system of linear equations. This method is applied to the analysis of hydroelastic FSI systems with complex boundary conditions that would be difficult or otherwise impossible to analyse using standard Galerkin methods. Specifically, the complex cases of inhomogeneous and discontinuous compliant wall properties and arbitrary hinge-joint conditions along the compliant surface are considered.

Introduction

Numerical methods are used to investigate the stability of a finite-length compliant wall interacting with an incompressible, high-Reynolds number, boundary layer flow over one side. In the limit of infinite Reynolds number, the flow may be modelled using an inviscid approximation. A schematic of the fluid-structure system is presented in Figure 1. The compliant wall is composed of a simple elastic plate that may have an added spring foundation and structural damping.

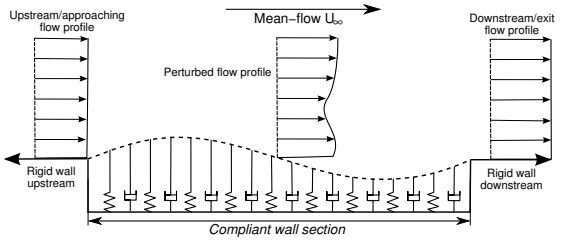

Figure 1: Schematic of the flow-structure system studied; the spring and dashpot foundations are absent for an unsupported elastic plate.

The problem of a one-sided *infinitely-long* compliant wall interacting with an inviscid flow is well documented through theoretical studies by Carpenter and Garrad [1].

This paper presents a technique whereby the fluid-structure system for a finite wall is represented as a single governing set of linear equations. Some simple results will be presented that may be validated against existing results obtained through theoretical or Galerkin methods. Finally, the new method will be used to perform an illustrative investigation into the complex wall behaviour with more complex inhomogeneous conditions and multiple hinged boundary conditions imposed.

System equations

The linear motion of the compliant wall is governed by the two-dimensional beam equation. Extra terms are added to account for the addition of homogeneous backing springs ($K\eta$) and uniform dashpot-type damping ($d\partial\eta/\partial t$) to model the effects of energy dissipation in the wall structure.

$$\rho_m h\frac{\partial^2\eta}{\partial t^2}+d\frac{\partial\eta}{\partial t}+B\frac{\partial^4\eta}{\partial x^4}+K\eta=-\Delta p(x,0,t)\ , \qquad (1)$$

where $\eta(x,t)$, ρ_m, h and B are, respectively, the plate's deflection, density, thickness and flexural rigidity, while $p(x,y,t)$ is the unsteady fluid pressure. In the present problem we apply hinged-edge conditions at the leading and trailing edges of the plate although in the method that follows there is no necessary restriction on such boundary conditions.

The fluid is modelled using the assumptions of incompressible and irrotational flow. This is an appropriate approximation for the high Reynolds number flow outside the boundary layer, however rotationality and viscous effects of the boundary layer are ignored. This therefore implies the approximation that the boundary layer is thin with respect to the wall disturbance wavelength and amplitude. A velocity perturbation potential $\phi(x,y,t)$ which satisfies Laplace's equation is introduced and the solution of which is then used in the linearised unsteady Bernoulli equation,

$$\Delta p=-\rho\frac{\partial\phi}{\partial t}-\rho U_\infty\frac{\partial\phi}{\partial x}\ , \qquad (2)$$

where ρ and U_∞ are, respectively, the fluid density and flow speed. The plate and fluid motions are coupled through the boundary condition of zero normal velocity at the wall and a balance of unsteady pressure forces.

Eigenvalue Determination

A Single Governing Equation for the System

Where Lucey and Carpenter [2] used an explicit time-marching scheme for the solution of the wall position, the objective here is to avoid temporal discretisation by direct solution of a single set of ordinary differential equations. The compliant wall position, $\eta(x,t)$, will be the single resulting variable.

Due to the linearity of Laplace's equation, the boundary element solution for the fluid equation may be expressed as the sum of a mean flow plus a distribution of singularities along the deforming compliant wall. In this case, zero order linear source(-sink) elements are chosen for the singularities, with the strength of each element denoted $\sigma(x)$. With the discretisation of the compliant surface into N elements, each with constant strength σ_i, the vector of element strengths may be determined through a